



An objective procedure for rainy season onset and withdrawal dates over the Mexico Valley Basin

Rodrigo Muñoz-Sánchez^{1,2} · Paulina Ordoñez^{1,3} · David Gallego³ · Carlos A. Ochoa-Moya¹

Received: 25 May 2023 / Accepted: 19 October 2023 / Published online: 2 November 2023
© The Author(s) 2023

Abstract

This work aims to define a procedure to declare rainy season onset and withdrawal dates for the Mexico Valley Basin, located in central Mexico. The onset/withdrawal is obtained using only precipitation for the study period 1981–2020. The onset is defined as the first day, between May 1st and July 15th, of the first 20 consecutive days having a 20-day average precipitation over the Basin of at least 2.5 mm/day. The withdrawal is defined as the last day, between September 1st and November 15th, of the last 20 consecutive days having a 20-day average precipitation of at least 1.7 mm/day. The mean onset is June 6th, with a standard deviation of 14.3 days; the mean withdrawal date is October 15th, with a standard deviation of 16.1 days; and the average length of the rainy season is 131 days, with a standard deviation of 22.7 days. These criteria maximize the precipitation change slope during onset/withdrawal. We categorized pre- and post-onset/withdrawal periods to investigate mean circulation characteristic changes. Besides a stark increase (decrease) in rainfall over the Basin during onset (withdrawal), we found that vertically integrated moisture transport over the Caribbean Low-Level Jet core region increases (decreases). The onset/withdrawal dates derived show interannual trends, while a late (early) withdrawal is associated with a positive (negative) ENSO Index, and a strong (weak) Caribbean Low Level Jet (CLLJ) is associated with a late (early) onset.

1 Introduction

The Mexico Valley Basin (MVB) is an elevated basin located in the center of the country (19.1°N – 20.8°N and 98.2°W – 99.8°W (black contour in Fig. 1)) (Conabio 2022). It houses one of the largest urban complexes in the world, the megalopolis of Mexico City and its Metropolitan Area,

with a population of 25.4 million as of 2017, but the basin also includes some extension of rural land.

The MVB is an endorheic basin whose urbanization led to the drying of the original lakes (Alcocer and Williams 1996). Groundwater extraction expanded significantly in the 1940s and provided enough water to supply the inhabitants of Mexico City until the mid-1960s (Ramírez 1990). Today, the aquifers are overexploited and depleted (Aguirre Gómez 2010), and the uncontrolled urban sprawl toward the mountain limits water infiltration to the subsoil and the aquifers' recharge. According to the global climate change vulnerability index (Imta 2015), the MVB presents a very high degree of vulnerability since, in conjunction with the water scarcity, the basin faces other issues such as significant environmental degradation caused by deforestation, soil erosion, loss of terrestrial and aquatic habitats, and river contamination (Montero-Rosado et al. 2022).

In the case of Mexico City, more anthropogenic changes have been produced in the last decades. The intense urbanization led to a significant urban heat island (UHI) effect (Jauregui 1993; 1997), which in turn has affected precipitation (Jauregui and Romales 1996). The timing of extreme precipitation events has shifted towards the evenings, with some evidence signaling the role of the UHI and the increase of anthropogenic aerosols in this change (Ochoa et al. 2015).

✉ Paulina Ordoñez
p.ordonez.perez@gmail.com

Rodrigo Muñoz-Sánchez
rodrigo.munoz@atmosfera.unam.mx

David Gallego
dgalpuy@upo.es

Carlos A. Ochoa-Moya
carlos.ochoa@atmosfera.unam.mx

¹ Instituto de Ciencias de la Atmósfera y Cambio Climático, Universidad Nacional Autónoma de México, Mexico City, Mexico

² Facultad de Ingeniería, Universidad Nacional Autónoma de México, Mexico City, Mexico

³ Departamento de Sistemas Físicos, Químicos y Naturales, Universidad Pablo de Olavide, Seville, Spain

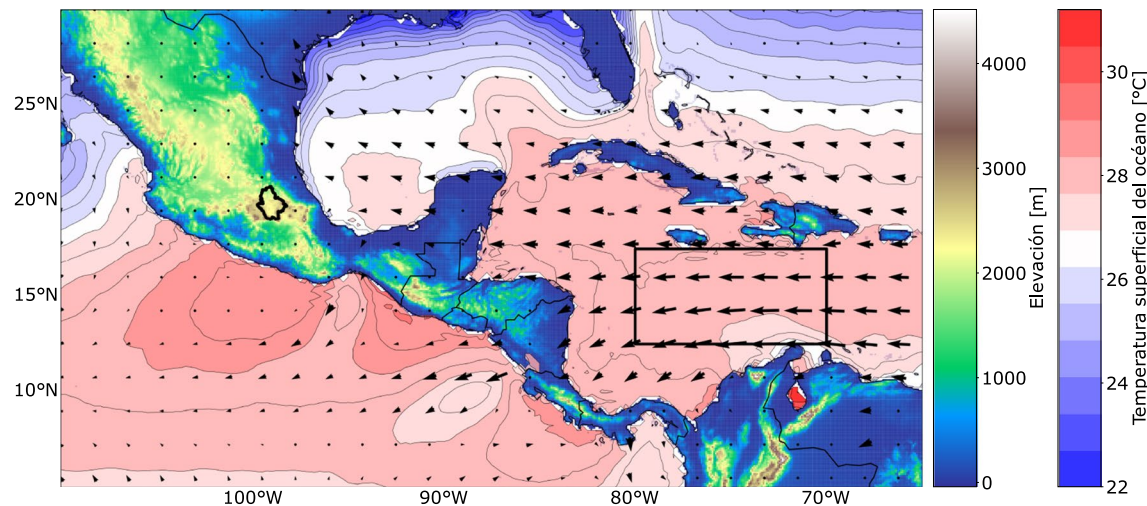


Fig. 1 Elevation, climatological mean sea surface temperature, and climatological mean wind in Mexico and the Caribbean. The Mexico Valley Basin is marked in central Mexico (black contour). The box in the Caribbean establishes the extent of the CLLJ core region

The occurrence of extreme events also has a spatial variability, with more intense rainfalls occurring in the western portion of Mexico City than in the eastern side, although this difference has been linked to orographic forcing and not to a more intense UHI effect (Magaña et al. 2003a).

The MVB has an average annual precipitation of 649 mm; it has a very small volume of dam storage and, as mentioned, it has high hydrological pressure (Conagua 2018). Half of the consumptive use corresponds to agricultural use, and the other half to drinking-water supply. Within the basin and with surrounding basins, water is transported from one source to another to serve the urban region (Montero-Rosado et al. 2022). The megalopolis suffers serious water-supply problems during years when the region experiences rainfall below average. This happened during the year 2021, when the government declared an emergency due to drought in several basins in the country including the MVB (Conagua 2021b). In the case of local agriculture, most of the irrigation is rainfed and depends heavily on the variability of the rainy season. Several production crops rely on the wet season onset besides the amount of rainfall during the season. In fact, years with late onsets — as the date is not predicted — have been reported to result in substantial crop losses along the entire Mexican territory (e.g., Rogé 2013; Granados et al. 2017). Water scarcity creates issues at the intersection of public policy, social development, and environmental degradation (Ávila García 2008; Lerner et al. 2018).

The Mexico Valley is subjected to a distinctively seasonal precipitation regime, with a rainy season typically starting in June and lasting up to late September (Fig. 2a), concentrating over 70% of the annual precipitation. A period lasting about 30 days of lower precipitation — the so-called midsummer drought (MSD) — is usually found within the rainy season

(Magaña et al. 1999; Herrera et al. 2015). It is typically characterized by two precipitation peaks in June and September, the second peak being usually smaller than the first one (Fig. 2a). This strong seasonality and especially the concentration of rainfall in the warmer half of the year led to some authors to include the MVB into the monsoon precipitation domain over North America (e.g., Wang and Ding 2008; Lee and Wang 2014; Wang et al. 2018). However, there is still some controversy about the actual extent of the North American Monsoon System (NAMS). This lack of agreement in the definition of the NAMS was recently reviewed by Ordoñez et al. (2019). These authors proposed a subdivision of the NAMS. In their scheme, the Northwestern Mexico and the Southeastern US regions (the classical core NAM region) were named as the Western North American Monsoon (WNAM). The WNAM is essentially characterized by a short monsoon season and a climatology associated with the variability of the wind over the Gulf of California. On the other hand, south and east of this region are central Mexico and the southern Pacific coast. This area is highly influenced by the Intertropical Convergence Zone and the Caribbean Low-Level Jet (CLLJ) (Fig. 1). It is worth mentioning that the IPCC recently slightly modified the definition of the NAMS in AR6 with respect to AR5. In this new regional domain for the NAM, the MVB is roughly in the limit (see figure AV.1 in IPCC 2021).

Beyond the discussion about whether the MVB region can be considered a monsoonal regime or not, this region can benefit from the prediction of the rainy season's onset and withdrawal. In this paper, as a first step, we focused on the determination of the onset and withdrawal of the rainy season in the MVB region. Characterizing these dates is of utmost importance as they are critical within regions where agriculture is rainfed (Wang et al. 2009), since small changes

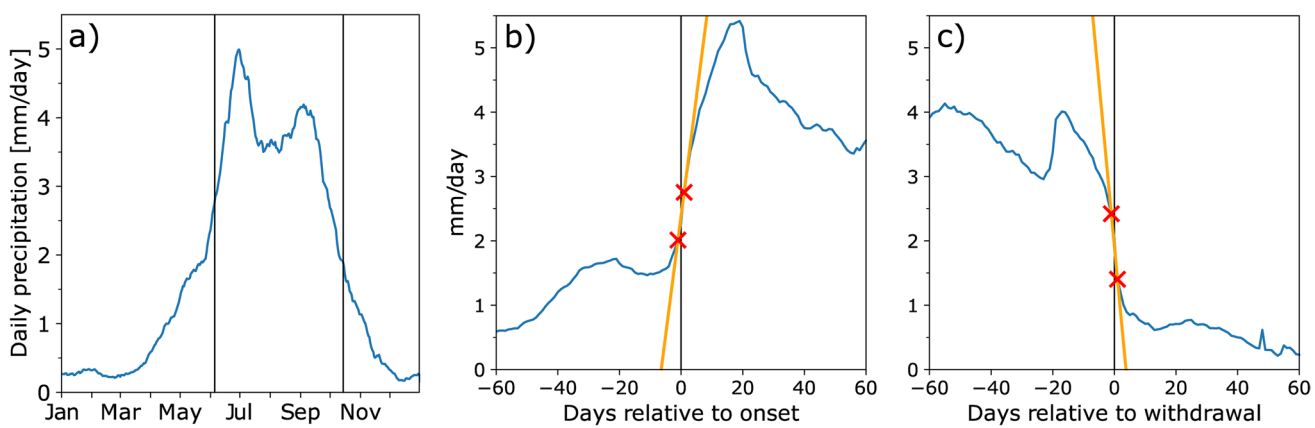


Fig. 2 Precipitation in the Mexico Valley Basin. **a** Mean annual cycle of 20-day running mean daily precipitation for the 1981–2020 study period. The daily precipitation has been averaged over a 20-day window. The vertical lines indicated the mean onset and withdrawal dates, as calculated in this paper. **b** Composite of precipitation around

the onset date. **c** Composite of precipitation around the withdrawal date. The red marks indicate the daily precipitation 1 day before and 1 day after the onset/withdrawal; the orange line represents the approximation of the slope of the precipitation evolution around the onset/withdrawal date, as explained in the text

in the onset's timing may significantly affect vulnerable populations (Raju et al. 2007). In this sense, Higgins et al. (1999) characterized the northwest and southwest Mexico warm season precipitation regime including the onset and withdrawal. A few published studies have determined the typical start of the rainy season in the global domain (Janowiak and Xie 2003; Zeng and Lu 2004) and at the present, the Mexican Water Authority (CONAGUA) declares the beginning of the rainy season as the climatological date of the beginning of the hurricane season (Conagua 2021), even though hurricanes do not represent the majority of the region's warm season precipitation (Dominguez and Magaña 2018; Dominguez et al. 2020). Despite these efforts, to the best of our knowledge, there have been no studies trying to estimate a rainy season onset and withdrawal specifically in the MVB. In this study, we have aimed to define an objective procedure for the declaration of onset and withdrawal dates in the Mexico Valley Basin on a year-to-year basis.

In the following, Section 2 describes the datasets and methods. Section 3 presents the onset and withdrawal time series, studies the spatial representativeness of the procedure, analyses the evolution of the large-scale circulation associated with the onset/withdrawal, and investigates the relationship and effect of ENSO on their interannual variability. Section 4 is a summary where the interannual variability and its mechanisms are further discussed.

2 Data and method

Whereas regional onset definitions focus on the migration of large scale atmospheric features in a region (Fitzpatrick et al. 2015), local onset definitions almost exclusively define a

monsoon onset in terms of the exceedance of a given threshold of local precipitation (e.g., Ananthakrishnan et al. 1967; Ahmed and Karmakar 1993; Marengo et al. 2001; Janowiak and Xie 2003; Pai and Rajeevan 2009; Diaconescu et al. 2015; Fitzpatrick et al. 2015; Asakereh et al. 2023; Misra et al. 2023; Omay et al. 2023; Oo 2023; among others). The reversal of the wind has also been used to determine the onset in the Indian summer monsoon (Joseph et al. 2006; Ordoñez et al. 2016, Wang et al. 2009). However, the North American monsoon does not exhibit a reversal in absolute wind direction, so we have based our method exclusively on precipitation.

For this study, precipitation data were obtained from the CHIRPS (Climate Hazards Infrared Precipitation with Stations) Database (<https://www.chc.ucsb.edu/data/chirps>; Funk et al. 2015). This database was chosen because it relies solely on observational information (satellites and precipitation gauges), has a high spatial resolution ($0.05^\circ \times 0.05^\circ$), and has proved reliable over Mexico (Perdigón-Morales et al. 2018). The study period contains 40 years from 1981 to 2020.

As mentioned above, the principal characteristic of the monsoon arrival is a fast change in precipitation, as it also occurs in the MVB; the withdrawal is usually less abrupt but still noticeable (Ahmed and Karmakar 1993; Ordoñez et al. 2016). It is relevant to note that as in other monsoonal regimes, the MVB is relatively frequent to have sudden increases in precipitation not related to the beginning of the monsoonal season but to the occurrence of short-term atmospheric disturbances. These are known as “bogus” onsets (Ordoñez et al. 2016). A similar situation can occur in the case of the withdrawal. To filter bogus onsets or withdrawals, we first computed the 20-day running mean of all

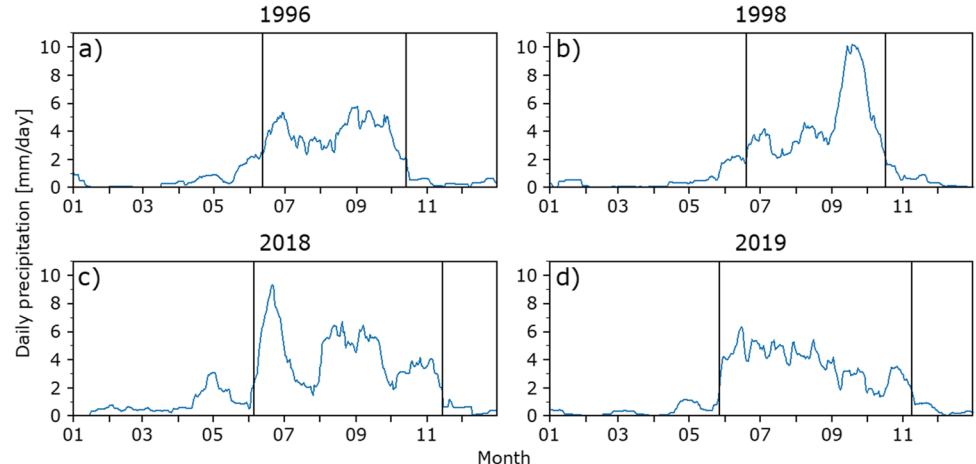
the climatic series considered, a technique which has proved effective in other regions (Ordoñez et al. 2016).

In order to build an objective procedure to define the onset in the MVB we designed an algorithm aimed to locate the dates when, a fast increase in precipitation results in a sustained rainy season. The withdrawal is defined when the sustained high-precipitation regime is interrupted by a fast enough decrease in precipitation. Therefore, we aim to look for precipitation thresholds exceeding certain values concurrently with the occurrence of large trends in the daily precipitation. Calling the smoothed precipitation series P (expressed in mm/day), the onset is defined as the first date where a given threshold P_o of this time series is exceeded for at least 20 consecutive days. Analogously, the withdrawal date is defined when a certain value P_w is last exceeded after being above it at least for the previous 20 days. The precipitation series P is averaged over the period 1981–2020 (Fig. 2a), and new composite precipitation series was calculated for $P_{o,k}=1, \dots, 4$ mm/day as day 0 (onset day) with $k=30$ steps of 0.1 mm/day, and for $P_{w,k}=1, \dots, 4$ mm/day as day 0 (withdrawal date) with $k=30$ steps of 0.1 mm/day. The optimal thresholds P_o and P_w are determined by locating the maximum in the absolute value of the slope of the precipitation series between May 1 and July 15 for P_o and between September 1 and November 15 for P_w . The slope in day d is estimated as the difference in the daily precipitation in day $d+1$ and $d-1$ as $m = \frac{P_{d+1} - P_{d-1}}{2}$ (expressed in mm/day $^{-2}$). We obtained a maximum increase in precipitation per day of $m=0.37$ mm/day 2 with the onset defined by a threshold $P_o=2.5$ mm/day (Fig. 2b). The threshold to define the withdrawal was found to be $P_w=1.7$ mm/day (Fig. 2c) with a decrease in precipitation of 0.5 mm/day 2 . Interestingly, the obtained thresholds are similar to those obtained by Higgins et al. (1999) for southwestern Mexico. The pre-rainy season and post-rainy season periods are distinguished by a near-zero slope (Fig. 2b and c).

As an example of the performance of our method under different circumstances, in Fig. 3, we show the cases of 1996, 1998, 2018, and 2019. The case of 2018 (Fig. 3c) corresponds to a typical humid season at the MVB, as it exhibits a precipitation peak right after the onset, followed by the MSD and, finally, a secondary increase in precipitation. The case of 1998 (Fig. 3b) also shows the MSD period, but in this example, the second precipitation peak is considerably larger than the first one. In 1996 (Fig. 3a), both precipitation peaks are similar. Finally, the 2019 precipitation evolution (Fig. 3d) shows the case of a year without the presence of the MSD. The onsets and withdrawals computed with our method are marked in Fig. 3 (black vertical lines). It is worth noting that the method can locate both onset and withdrawal dates under different atmospheric conditions. There are years in which the withdrawal date is more clearly defined, such as in 2019. However, in other years, the precipitation shows relatively fast increases not related to the rainy season but associated with short-lived synoptic disturbances, as in 2018. Our results suggest that even for these cases of bogus onsets, the methodology is robust.

Apart from precipitation data, the ERA5 reanalysis (Hersbach et al. 2020) from the European Centre for Medium-range Weather Forecasts (ECMWF) has been used to obtain climatological fields such as the vertically integrated moisture flux (VIMF) and the zonal and meridional wind components related to the occurrence of the onset and the withdrawal. To characterize the strength of the CLLJ, we computed standardized anomalies of the zonal ERA5 wind at 925 hPa with respect to the 1981–2010 climatology in the CLLJ core region, defined as the zone between 12.5°–17.5°N and 70°–80°N (Wang 2007; Cook and Vizy 2010). ENSO has been characterized by the NINO4 index (NCEI 2022) (<https://www.cpc.ncep.noaa.gov/data/indices/sstoi.indices>), which considers SST exclusively.

Fig. 3 Evolution of daily precipitation for four selected years. The daily precipitation has been averaged over a 20-day window. The vertical lines mark the onset and withdrawal dates for each year



3 Results

3.1 Time series analysis

The time series of the onset and withdrawal are presented in Fig. 4. Both the start and the end of the rainy season in the MVB show high variability. A 5-year moving average of the onset/withdrawal time series (orange lines in Fig. 4) reveals periods with a slight tendency to earlier onsets and withdrawals as around the mid-1980s and around 2010. For the period 1981–2020, we found an average onset of June 6, with a standard deviation of 14.3 days; the earliest onset date is May 9, and the latest occurred on June 26. The mean withdrawal date occurs on October 15, with a standard deviation of 16.1 days; the earliest withdrawal is September 14, and the latest is November 14. The average length of the rainy season was of 131 days, with a standard deviation of 22.7 days. Between 1981 and 2020, the shortest rainy season was 91 days long, and the longest one 192 days long. The average onset and withdrawal dates have been represented in Fig. 1a to ease comparison with the average annual precipitation cycle of the study area.

3.2 Representativeness of the procedures

The representativeness of the procedures was analyzed by constructing a composite around the onset/withdrawal date and evaluating the evolution of the precipitation by representing the average precipitation in 3-day periods before and after the onset/withdrawal date (Fig. 5). It is apparent from Figure a and b that the southwestern and southeastern parts of the basin receive rainfall (~ 4 mm/day) prior to the onset, which is likely a result of the orography on these areas. After the onset (Fig. 5c), rainfall intensifies in both areas (more than 6 mm/day), and all the MVB begins to receive moderate rainfall. Several days after the onset (Fig. 5d), the rainfall over the basin has clearly increased significantly.

A clear rainfall retreat centered on the rainy season withdrawal over the MVB can be ascertained from Fig. 6. Within 1 to 6 days before the withdrawal over the MVB, rainfall spreads over the basin with amounts ranging from 2 to more than 4 mm/day (Fig. 6a and b). The withdrawal is clearly manifested with a generalized receding of rainfall in the MVB (Fig. 6c) which exhibits a rain rate of about 1 mm/day, slightly greater over the southeastern and southwestern mountain ranges than in the valley. Several days after withdrawal, the rainfall over the basin is quite low (Fig. 6d).

Fig. 4 Time series for the onset and withdrawal dates. The blue (green) line and dots represent each year's onset (withdrawal) date, while the orange one is the five-year mean. The solid horizontal line is the mean onset/withdrawal date, and the dotted lines mark one and two standard deviations from the mean

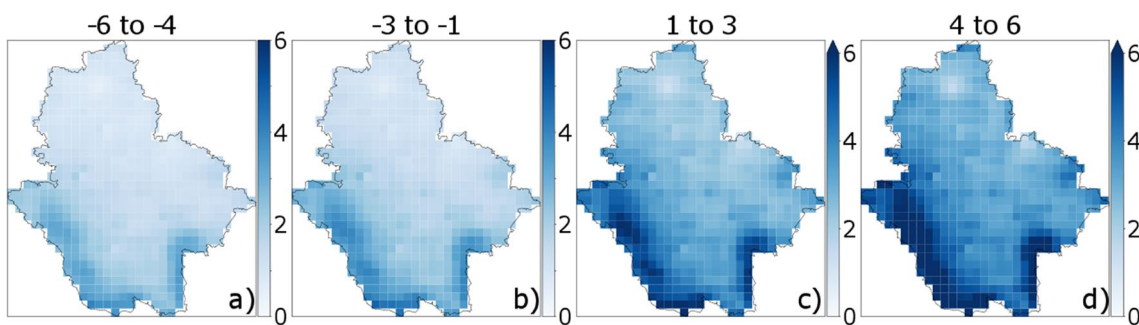
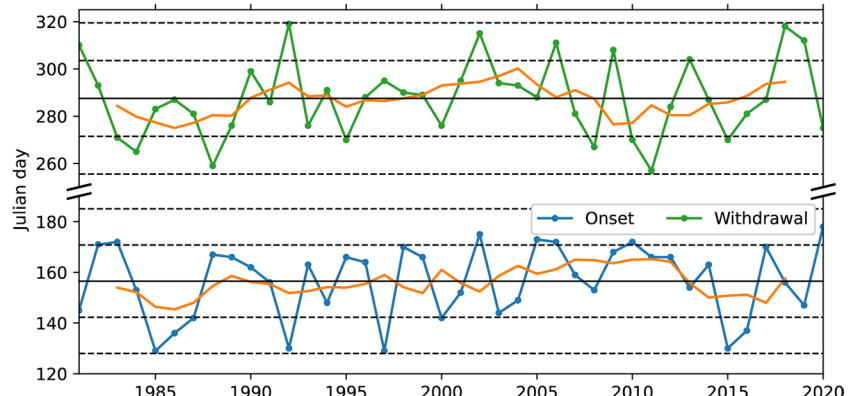


Fig. 5 Composite evolution of the spatial distribution of precipitation over the MVB prior to and after the onset at intervals of 3 days for **a** days –6 to –4 prior to the onset, **b** days –3 to –1 prior to the onset, **c**

days 1 to 3 after the onset, and **d** days 4 to 6 after the onset. The color bar represents the daily precipitation in millimeters per day

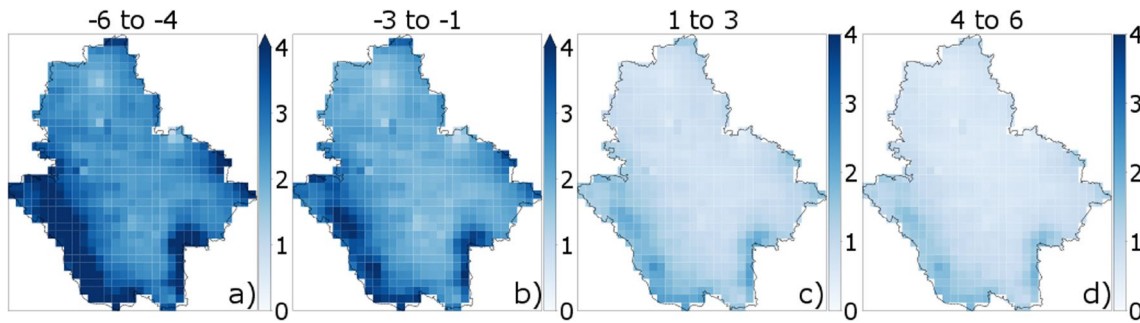


Fig. 6 Composite evolution of the spatial distribution of precipitation over the MVB prior to and after the withdrawal at intervals of 3 days for **a** days -6 to -4 prior to the withdrawal, **b** days -3 to -1 prior to

the withdrawal, **c** days 1 to 3 after the withdrawal, and **d** days 4 to 6 after the withdrawal. The color bar represents the daily precipitation in millimeters per day

Both Figs. 5 and 6 clearly show that the larger precipitation changes occur around the onset/withdrawal selected by our algorithm (Figs. 5c and 6c), followed by lower changes 6 days before or after the date of the onset or withdrawal. Although some regions of the basin are rainier than others — especially the southwestern portion — it is evident that both the onset and withdrawal occur homogeneously across the whole basin. Such behavior indicates that the definition of a single onset and withdrawal date for the whole basin is meaningful.

3.3 Characterization of the large-scale circulation associated with the onset/withdrawal

To better understand the processes related to the onset and withdrawal of the rainy season, we examined the evolution of the moisture advection before and after both events by

computing the composite of the VIMF and the difference between the fields during onset/withdrawal (day 0 of each composite) with the average of 3-day periods before and after the withdrawal date.

Figure 7 shows the 40-year composite sequence of VIMF anomalies with respect to the onset (day 0) for two triads before and another two after the onset. About two triads before the onset northwestern VIMF anomalies are present in the CLLJ region (Fig. 7a and b) and the Great Plains Low Level Jet (Danko and Martin 2018). Anomalies of the zonal wind at the eastern tropical North Pacific are eastern (negative) with respect to the mean moisture advection implying a deceleration of the average flow (see Fig. 2). After the onset, stronger eastern low-level winds prevail around the CLLJ region (Fig. 7c and d) and the prevalence of the westerly component of the flow over the tropical eastern North Pacific is also evident. This

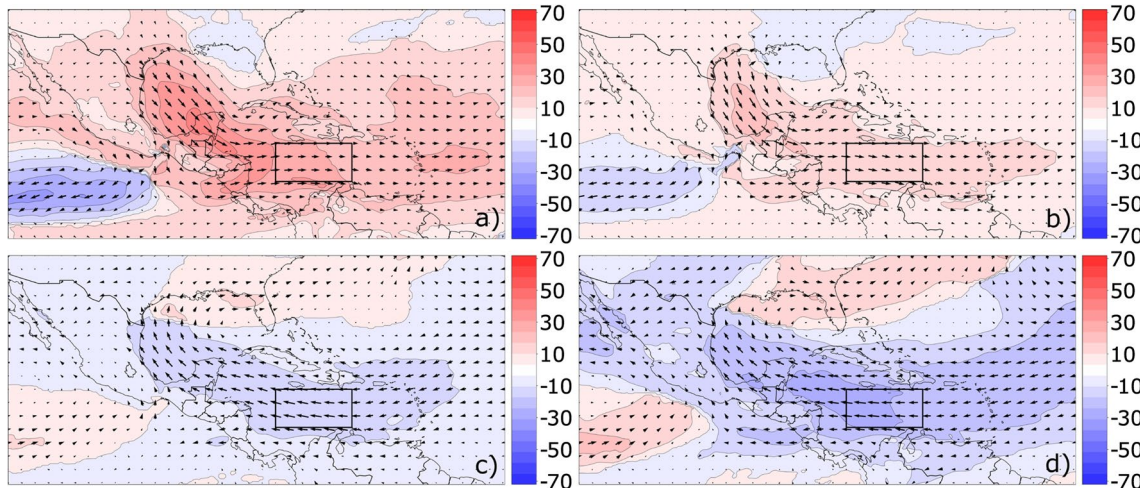


Fig. 7 Composite of vertical integral of moisture flux (VIMF) around the onset date. Difference between onset date and averages of 3 days: **a** days -6 to -4 , **b** -3 to -1 , **c** 1 to 3, and **d** 4 to 6. The color bar indicates the water vapor flux, and its unit is in kilograms per meter

second. Shading indicates the sign of the zonal anomaly: Red is a westerly anomaly, and blue is an easterly one. The box in the Caribbean establishes the extent of the CLLJ core region

configuration favors moisture convergence over central Mexico.

Figure 8 represents the case of the withdrawal. The situation before the withdrawal is similar to that observed after the onset (Fig. 8a and b), with enhanced moisture advection carried by the CLLJ and an intense flow toward southern Mexico over the tropical eastern North Pacific. After the withdrawal, the moisture flux noticeably changes (Fig. 8c and d) with moisture flux anomalies low over the CLLJ region. A wind anomaly dipole is present over the North Atlantic, suggesting a northern displacement of the North Atlantic Subtropical High immediately after the withdrawal. VIMF anomalies over the Pacific in front of the southern Mexico coast also present an opposite sign than before the withdrawal.

The evolution of VIMF divergence averaged over the MVB around the onset/withdrawal (not shown) corresponds well with the precipitation evolution. Before the onset, the VIMF divergence has an average value in the study area of $-1.25 \text{ kg/m}^2 \text{ day}$, which changes to $-4.25 \text{ kg/m}^2 \text{ day}$ the day after the onset. These values closely correspond to the changes in the average precipitation around the onset and the withdrawal. Figure 2 shows that the average daily precipitation before the onset is around 1.5 mm/day and that it stabilizes to around 4 mm/day after the onset. For the withdrawal, the VIMF changes from $-3.5 \text{ kg/m}^2 \text{ day}$ to $1.0 \text{ kg/m}^2 \text{ day}$ the day before and after the withdrawal date; this moisture availability is consistent with the average precipitation change of 3.5 mm/day before and 0.75 mm/day after the withdrawal date (Fig. 1c). The resemblance between the VIMF over the MVB and the daily precipitation around the onset/withdrawal stresses the relevance of

the regional changes in the VIMF in relation to the rainy season in the MVB.

3.4 Trends and interannual variability

We performed a sliding trend analysis using a 20-year window for the 5-year moving average time series. Ordinary least squares regression is used, which is simpler than other trend detection methods but yields similar results (Hess et al. 2001); additionally, it is ideal since no seasonality correction is needed. Linear regressions were fitted to each subperiod. The interannual variability of the resulting time series were also analyzed by calculating the sliding Pearson correlation between the onset/withdrawal series and each of the monthly El Niño-Southern Oscillation (ENSO) and the Caribbean Low-Level Jet (CLLJ) indexes. Significance of the sliding trends and the Pearson correlation coefficients were tested using a bootstrapping method with 10,000 resamples. Bootstrapping is a non-parametric sampling method that does not require normality in the distributions (Lunneborg 1985).

Figure 9 shows the results of linear regressions for each subperiod of 20-year windows, where the years on the x-axis mark the middle year of the sliding window. In this figure, the corresponding trends in precipitation during the wet summer season are also included. Our results show a significant increase between 0.3 and 0.7 days/year for the onset date from 1988 to 1999. The trend peaks in 1997 and then declines. The withdrawal shows an increasing trend with a slope between 0.4 and 1.0 days/year from 1988 to 1995, with a maximum in 1990. Subsequently, there is a decreasing trend of around 0.5 days/year from 2001 to 2004. These changes result in an increasing trend of the length of the

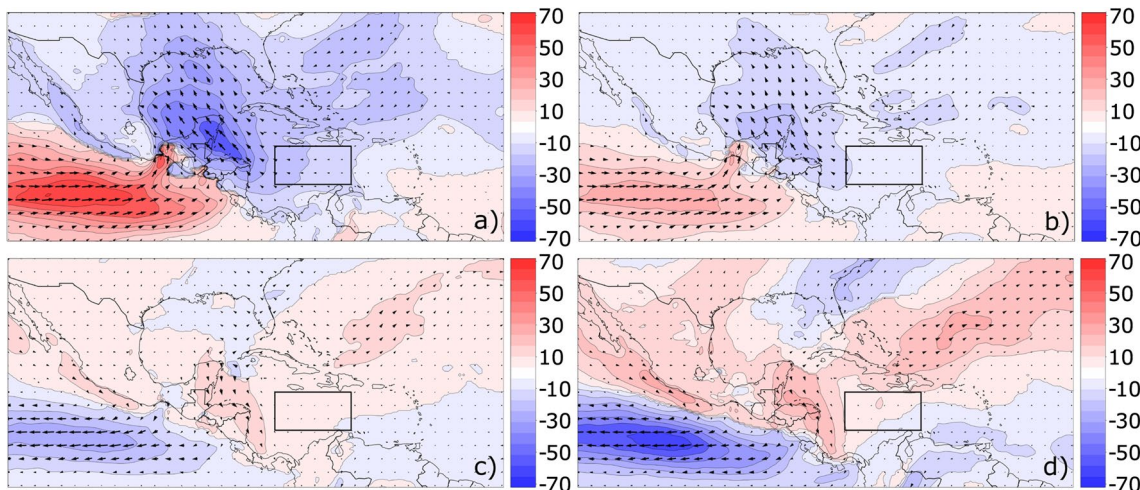


Fig. 8 Composite of vertical integral of moisture flux (VIMF) around the withdrawal date. Difference between onset date and averages of 3 days: **a** days -6 to -4 , **b** -3 to -1 , **c** 1 to 3 , and **d** 4 to 6 . The color bar indicates de water vapor flux, and its unit is in kilograms per

meter second. Shading indicates the sign of the zonal anomaly: Red is a westerly anomaly, and blue is an easterly one. The box in the Caribbean establishes the extent of the CLLJ core region

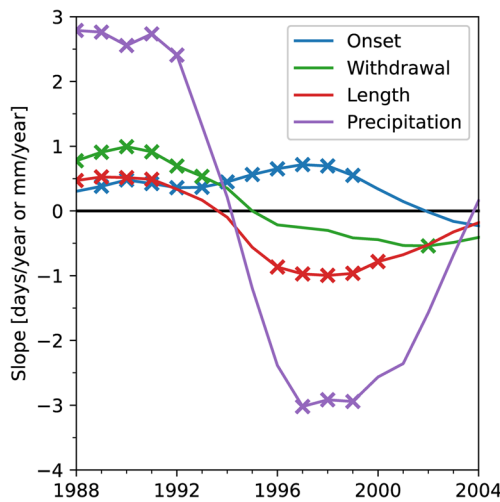


Fig. 9 Linear trends for 20-year periods for the onset, withdrawal, rainy season length (withdrawal date — onset date), and the precipitation amount between the onset and withdrawal. The horizontal axis represents the central year of the 20-year period where the trend was evaluated. Crosses indicate significant trends ($p < 0.025$)

rainy season of around 0.5 days/year from 1988 to 1991, and a decreasing trend between 0.6 and 1.0 days/year from 1995 to 2001, with a maximum decreasing trend in 1998. The analysis of the rainy season precipitation series reveals an increasing trend of 2.7 mm/year in the periods around 1988–1992, and a negative trend in the late 1990s and early 2000s, reaching statistically significant values ($p < 0.025$) of 3 mm/year from 1997 to 1999. When the trend is evaluated over a 40-year window, no statistically significant trend occurs throughout the entire study period.

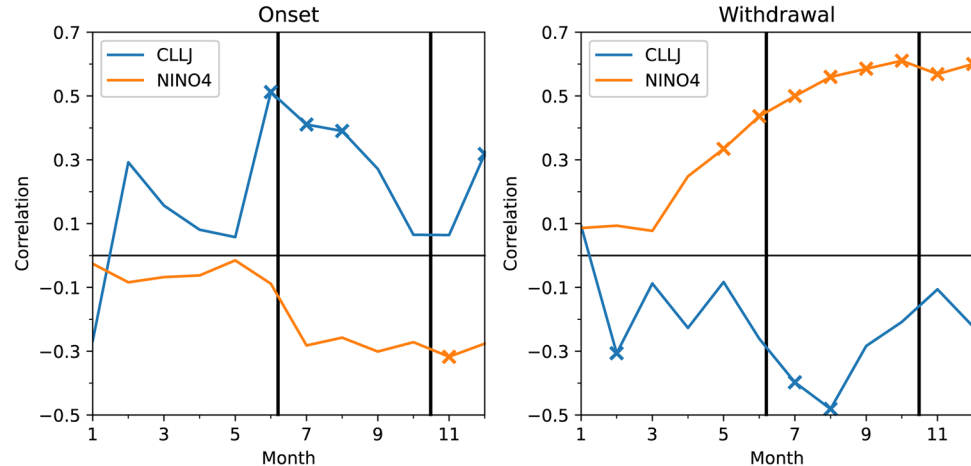
Finally, we calculated the Pearson correlations between the onset/withdrawal and ENSO as quantified by the NINO4 index. The CLLJ has been shown to be relevant to precipitation in Central Mexico (Wang 2007; Cook and Vizy 2010; Perdigón-Morales et al. 2021), so the correlation has also

been evaluated with the strength of the CLLJ, quantified as the anomaly of the zonal wind as described in Section 2. We computed the Pearson correlations for the index values corresponding to the 12 months of the same year of the onset/withdrawal (Fig. 10). Our results suggest that ENSO has very little influence on the onset date, as the values of the correlation prior to the onset are low and non-significant. Correlations of the onset date with the strength of the CLLJ are positive and significant around the onset, suggesting that a stronger CLLJ is related to a slightly delayed onset. For the withdrawal, correlations with the NINO4 are significant with values around 0.3 to 0.6 between March and August, indicating that a warming (cooling) of the tropical Pacific during the months before the withdrawal is related to late (early) ends of the rainy season. Concerning the CLLJ index, the correlations are in general negative, but they only reach statistical significance in July and August, prior to the withdrawal occurrence ($r = -0.40$ and $r = -0.48$, respectively).

4 Summary and discussion

The Mexico Valley Basin is home to more than 25 million inhabitants, who strongly depend on rainfall both for human water consumption and agriculture, so the precise characterization of the precipitation, particularly the onset and withdrawal of the rainy season is of paramount social importance. In this work, we have shown that by using time-smoothed high-resolution precipitation data, it is possible to define an onset procedure for the MVB as the first day of the first 20-day streak with precipitation of at least 2.5 mm/day. For the withdrawal, we followed an analogous approach, and it has been defined as the last day of the last 20-day streak with precipitation of at least 1.7 mm/day. These thresholds were chosen after a calibration procedure aimed to maximize the rate of change in the precipitation around the onset/withdrawal. Based on this method, we found that for the period

Fig. 10 Lagged correlations between the onset/withdrawal time series and the monthly value of the El Niño4 and the CLLJ index for the same year. The black vertical lines indicated the mean onset and withdrawal dates. Crosses indicate statistical significance ($p < 0.05$)



1981–2020, the average onset occurs on June 6 and the average withdrawal on October 15, implying a typical duration of the rainy season of 131 days.

Our results show that both onset and withdrawal capture quite well the fast increase and decrease in precipitation in the study area characteristic of the start and end of the rainy season (Figs. 5 and 6). The analysis of the changes in the moisture flux toward the Mexican Valley Basin shows that during the wet season onset (withdrawal), there is a clear and fast strengthening (weakening) of the moisture flux on the exit of the CLLJ core region, through the Yucatan peninsula, and into central Mexico. Our results agree with Cook and Vizy (2010), who found that from May to September, moisture is lost to the Caribbean basin and transported by the zonal flow to Central America. The rainy season onset is concurrent with a strong inward moisture flow from the Pacific Ocean converging on the Isthmus of Tehuantepec, located on the southern coast of Mexico. On the contrary, the withdrawal is associated with an outward moisture flux in this area. In our knowledge, this dynamical feature has not been associated before with the timing of the onset/withdrawal of the wet season in central Mexico.

Both onset and withdrawal exhibit large interannual variability in the Mexico Valley Basin. Between 1981 and 2020, the earliest onset occurred on May 9 (1985, 1997) and the latest on June 26 (2020). The range of dates for the withdrawal is quite large as well, as 2011 was the earliest in our study period (September 14); in 1992, the end of the rainy season did not happen until November 14. There is not a significant tendency in the onset/withdrawal dates in the 40-year study period. However, trends of 20 years moving window revealed that the withdrawal dates were slightly but significantly delayed between 1988 and 1994 at a rate of around 1 day per year, while between 1995 and 2002, there is a change in the sign of the tendency, with a small trend toward earlier withdrawals. In the case of the onset, in general, we found positive significant trends for almost all the entire study period (i.e., a tendency to later onsets) that was larger during 1995–2002, reaching values of around 0.5 days per year. Due to the trends in the onset and withdrawal dates, the length of the rainy season at Mexico Valley Basin oscillated significantly during the study period. This is evidenced by the positive trends in the length of the rainy season between 1988 and 1994 followed by a significant negative trend in the duration between 1994 and 2002. In the case of the first period, the increase in the length of the rainy season was due to a delay in the rainy season withdrawal. For the second period, the decrease in the length of the rainy season was due both to later onsets and earlier withdrawals. Interestingly, the trends in rainy season precipitation closely follow those of the length of the rainy season, implying that a longer rainy season is also a wetter one, and suggesting that the physical drivers related to the length of the rainy

season can be also related with the precipitation amount in the MVB.

We found large and significant positive Pearson correlations between the NINO4 index and the withdrawal date since May. By contrast, we did not find a significant relationship between the onset of the rainy season and ENSO. The positive correlation with the withdrawal implies that warmer temperatures over the tropical Pacific in summer (El Niño developing conditions) are related to a late withdrawal and vice versa. As such, El Niño conditions promote an extended rainy season that stretches well into early autumn. While this extended season may have a larger total rainfall, it does not necessarily mean that the summer precipitation is also higher during El Niño conditions, since the excess rainfall may be associated with a late withdrawal (Fig. 6).

Even though the correlation is found in the middle of summer, precipitation anomalies associated with ENSO take 3 to 6 months to reach the Americas. This delay in the correlation agrees with the atmospheric bridge theory (Alexander et al. 2002), which established a link between SST anomalies in the equatorial Pacific with those in the Tropical Atlantic, approximately 3–6 months following the peak in tropical Pacific SST anomalies. One such mechanism that causes the teleconnection is that during El Niño events, there is a southward migration of the ITCZ, which causes a weakening of the trade winds over the tropical North Atlantic and the Caribbean, reducing surface evaporation and leading to higher SSTs (Klein et al. 1999; Giannini et al. 2001).

Among several factors that influence the strength of the CLLJ, Wang (2007) has identified the mechanism through which the SST modulates the zonal wind. In a classic Gill mechanism, an off-equatorial diabatic heating generates a cyclonic circulation northwest of the heating anomaly (Gill 1980), which decreases the strength of the North Atlantic Subtropical High, debilitating the CLLJ (Wang 2007; Wang and Lee 2007; Wang et al. 2007). Additionally, Wang (2007) found wind-precipitation correlations for Central Mexico that stressed that enhanced moisture flux divergence at the exit of the CLLJ core region decreases convection in Central Mexico and vice versa. Accordingly, El Niño (La Niña) conditions in summer would propagate (through the atmospheric bridge) over 3 to 6 months and cause positive (negative) SST anomalies in the Caribbean, leading to a weakening (strengthening) of the CLLJ around October and November, which in turn weakens (strengthens) moisture divergence in the exit zone of the CLLJ and enhances (suppresses) precipitation in Central Mexico and delays (advances) the withdrawal in the Mexico Valley Basin.

Finally, we also found significant changes in the length of the rainy season directly related to the variability of the wind in the CLLJ core region. For the onset, a strong (weak) CLLJ causes a late (early) onset, agreeing with the suppression of precipitation by a strong CLLJ in summer through the

enhancement of moisture divergence. The withdrawal date is negatively correlated with the summer CLLJ. Therefore, a weak (strong) CLLJ in summer causes a late (early) withdrawal. In this sense, a strong CLLJ during August leads to enhanced moisture divergence at the exit of the CLLJ core region. This might trigger an early withdrawal in September, thus modulating the withdrawal date and rainy season length.

Author contribution P.O. and D.G. conceived and designed the research. R.M.-S. developed the analysis and prepared the original draft. R.M.-S., P.O., D.G., and C.O.-M. reviewed and edited the manuscript. All authors have read and agreed to the published version of the manuscript.

Funding This research was funded by the project PAPIIT (DGAPA-UNAM) IN113222 “Predicción del inicio y fin de la temporada lluviosa en la Cuenca del Valle de México.” Paulina Ordoñez received the support of María Zambrano (UPO; Ministry of Universities; Recovery, Transformation and Resilience Plan — Funded by the European Union — Next Generation EU).

Data availability Data generated and analyzed during the current study will be made available by the authors upon request.

Declarations

Competing interests The authors declare no competing interests.

Open Access This article is licensed under a Creative Commons Attribution 4.0 International License, which permits use, sharing, adaptation, distribution and reproduction in any medium or format, as long as you give appropriate credit to the original author(s) and the source, provide a link to the Creative Commons licence, and indicate if changes were made. The images or other third party material in this article are included in the article’s Creative Commons licence, unless indicated otherwise in a credit line to the material. If material is not included in the article’s Creative Commons licence and your intended use is not permitted by statutory regulation or exceeds the permitted use, you will need to obtain permission directly from the copyright holder. To view a copy of this licence, visit <http://creativecommons.org/licenses/by/4.0/>.

References

- Adams DK, Comrie AC (1997) The North American Monsoon. *Bull Am Meteor Soc* 78(10):2197–2214. [https://doi.org/10.1175/1520-0477\(1997\)078%3c2197:TNA%3e2.0.CO;2](https://doi.org/10.1175/1520-0477(1997)078%3c2197:TNA%3e2.0.CO;2)
- Aguirre Gómez, R (2010) Estudios Sobre Los Remanentes de Cuerpos de Agua En La Cuenca de México; UNAM, Instituto de Geografía: Ciudad de Mexico, Mexico; ISBN 9786070219887
- Ahmed R, Karmakar S (1993) Arrival and withdrawal dates of the summer monsoon in Bangladesh. *Int J Climatol* 13(7):727–740. <https://doi.org/10.1002/joc.3370130703>
- Alcocer J, Williams WD (1996) Historical and recent changes in Lake Texcoco, a saline lake in Mexico. *Int J Salt Lake Res* 5(1):45–61. <https://doi.org/10.1007/BF01996035>
- Alexander MA, Bladé I, Newman M, Lanzante JR, Lau N-C, Scott JD (2002) The atmospheric bridge: the influence of ENSO teleconnections on air-sea interaction over the global oceans. *J Clim* 15(16):2205–2231. [https://doi.org/10.1175/1520-0442\(2002\)015<2205:TABTIO>2.0.CO;2](https://doi.org/10.1175/1520-0442(2002)015<2205:TABTIO>2.0.CO;2)
- Ananthkrishnan R, Achary UR, Ramakrishnan AR (1967) FMU Report No.1, IMD Forecasting Manual Part IV, 18, November
- Asakereh H, Masoodian SA, Tarkarani F, Zandkarimi S (2023) Decadal variations of the onset, cessation, and length of the widespread rainy season in Iran. *Theoret Appl Climatol* 152(1–2):599–615. <https://doi.org/10.1007/s00704-023-04378-4>
- Ávila García, P (2008) Vulnerabilidad socioambiental, seguridad hídrica y escenarios de crisis por el agua en México. *Ciencias*, 90, 46–57. Universidad Nacional Autónoma de México
- Bravo Cabrera JL, Azpiazu Romero E, Zarzalui Such V, Gay García C, Estrada Porrúa F (2010) Significance tests for the relationship between “El Niño” phenomenon and precipitation in Mexico. *Geofísica Internacional* 49(4):245–261
- Conabio (2022). Portal de Geoinformación 2022. <http://www.conabio.gob.mx/informacion/gis/>
- Conagua (2018). Estadísticas del agua en México. http://sina.conagua.gob.mx/publicaciones/EAM_2018.pdf. Last access: 23 November 2022
- CONAGUA (2021a). Reporte del Clima en México, 2020. <https://smn.conagua.gob.mx/tools/DATA/Climatolog%C3%A9tica/Diagn%C3%B3stico%20Atmosf%C3%A9rica/Reporte%20del%20Clima%20en%20M%C3%A9jico/Anual2020.pdf>. Last access: 23 November 2022
- CONAGUA (2021b). Publica Conagua acuerdo de inicio de emergencia por sequía para garantizar abasto de agua a la población. Available at: https://www.gob.mx/cms/uploads/attachment/file/661203/Comunicado_de_Prensa_0626-21.pdf. Last access: 23 November 2022
- Cook KH, Vizy EK (2010) Hydrodynamics of the Caribbean Low-Level Jet and its relationship to precipitation. *J Clim* 23(6):1477–1494. <https://doi.org/10.1175/2009JCLI3210.1>
- Danko JF, Martin ER (2018) Understanding the influence of ENSO on the Great Plains low level jet in CMIP5 models. *Clim Dyn* 51:1537–1558. <https://doi.org/10.1007/s00382-017-3970-9>
- Diaconescu EP, Gachon P, Scinocca J, Laprise R (2015) Evaluation of daily precipitation statistics and monsoon onset/retreat over western Sahel in multiple data sets. *Clim Dyn* 45(5–6):1325–1354. <https://doi.org/10.1007/s00382-014-2383-2>
- Dominguez C, Magaña V (2018) The role of tropical cyclones in precipitation over the tropical and subtropical North America. *Front Earth Sci* 6:19. <https://doi.org/10.3389/feart.2018.00019>
- Dominguez C, Done JM, Bruyère CL (2020) Easterly wave contributions to seasonal rainfall over the tropical Americas in observations and a regional climate model. *Clim Dyn* 54(1–2):191–209. <https://doi.org/10.1007/s00382-019-04996-7>
- Douglas MW, Maddox RA, Howard K, Reyes S (1993) The Mexican Monsoon. *J Clim* 6(8):1665–1677. [https://doi.org/10.1175/1520-0442\(1993\)006%3c1665:TMM%3e2.0.CO;2](https://doi.org/10.1175/1520-0442(1993)006%3c1665:TMM%3e2.0.CO;2)
- Ellis AW, Saffell EM, Hawkins TW (2004) A method for defining monsoon onset and demise in the southwestern USA. *Int J Climatol* 24(2):247–265. <https://doi.org/10.1002/joc.996>
- Fitzpatrick RGJ, Bain CL, Knippertz P, Marsham JH, Parker DJ (2015) The West African Monsoon onset: a concise comparison of definitions. *J Clim* 28(22):8673–8694. <https://doi.org/10.1175/JCLI-D-15-0265.1>
- Funk C, Peterson P, Landsfeld M, Pedreros D, Verdin J, Shukla S, Husak G, Rowland J, Harrison L, Hoell A, Michaelsen J (2015) The climate hazards infrared precipitation with stations—a new environmental record for monitoring extremes. *Sci Data* 2(1):150066. <https://doi.org/10.1038/sdata.2015.66>
- Giannini A, Chiang JCH, Cane MA, Kushnir Y, Seager R (2001) The ENSO teleconnection to the Tropical Atlantic Ocean: contributions of the remote and local SSTs to rainfall variability in the

- tropical Americas. *J Clim* 14(24):4530–4544. [https://doi.org/10.1175/1520-0442\(2001\)014%3c4530:TETTTT%3e2.0.CO;2](https://doi.org/10.1175/1520-0442(2001)014%3c4530:TETTTT%3e2.0.CO;2)
- Gill AE (1980) Some simple solutions for heat-induced tropical circulation. *Q J R Meteorol Soc* 106(449):447–462. <https://doi.org/10.1002/qj.49710644905>
- Granados R, Soria J, Cortina M (2017) Rainfall variability, rainfed agriculture and degree of human marginality in North Guanajuato, Mexico: rainfall variability in North Guanajuato. *Singap J Trop Geogr* 38(2):153–166. <https://doi.org/10.1111/sjtg.12191>
- Herrera E, Magaña V, Caetano E (2015) Air-sea interactions and dynamical processes associated with the midsummer drought. *Int J Climatol* 35(7):1569–1578. <https://doi.org/10.1002/joc.4077>
- Hersbach, H., Bell, B., Berrisford, P., Hirahara, S., Horányi, A., Muñoz-Sabater, J., Nicolas, J., Peubey, C., Radu, R., Schepers, D., Simmons, A., Soci, C., Abdalla, S., Abellán, X., Balsamo, G., Bechtold, P., Biavati, G., Bidlot, J., Bonavita, M., ... Thépaut, J. (2020). The ERA5 global reanalysis. *Quart J Royal Meteorol Soc* 146(730), 1999–2049 <https://doi.org/10.1002/qj.3803>
- Hess A, Iyer H, Malm W (2001) Linear trend analysis: a comparison of methods. *Atmos Environ* 35(30):5211–5222. [https://doi.org/10.1016/S1352-2310\(01\)00342-9](https://doi.org/10.1016/S1352-2310(01)00342-9)
- Higgins RW, Chen Y, Douglas AV (1999) Interannual variability of the North American warm season precipitation regime. *J Clim* 12(3):653–680. [https://doi.org/10.1175/1520-0442\(1999\)012%3c0653:IVOTNA%3e2.0.CO;2](https://doi.org/10.1175/1520-0442(1999)012%3c0653:IVOTNA%3e2.0.CO;2)
- Imta (2015). Atlas de vulnerabilidad hídrica en México ante el cambio climático. https://www.imta.gob.mx/biblioteca/libros_html/atlas-2016/files/assets/common/downloads/publication.pdf. Last access: 23 November 2022
- IPCC, 2021: Annex V: Monsoons [Cherchi, A., A. Turner (eds.)]. In Climate change 2021: the physical science basis. Contribution of Working Group I to the Sixth Assessment Report of the Intergovernmental Panel on Climate Change [Masson-Delmotte, V., P. Zhai, A. Pirani, S.L. Connors, C. Péan, S. Berger, N. Caud, Y. Chen, L. Goldfarb, M.I. Gomis, M. Huang, K. Leitzell, E. Lonnoy, J.B.R. Matthews, T.K. Maycock, T. Waterfield, O. Yelekçi, R. Yu, and B. Zhou (eds.)]. Cambridge University Press, Cambridge, United Kingdom and New York, NY, USA, pp. 2193–2204, <https://doi.org/10.1017/9781009157896.019>
- Janowiak JE, Xie P (2003) A global-scale examination of monsoon-related precipitation. *J Clim* 16(24):4121–4133. [https://doi.org/10.1175/1520-0442\(2003\)016%3c4121:AGEOMP%3e2.0.CO;2](https://doi.org/10.1175/1520-0442(2003)016%3c4121:AGEOMP%3e2.0.CO;2)
- Jauregui E (1993) Mexico City's urban heat island revisited. *Erdkunde* 47(3) <https://doi.org/10.3112/erdkunde.1993.03.03>
- Jauregui E (1995) Rainfall fluctuations and tropical storm activity in Mexico. *Erdkunde* 49:39–48
- Jauregui E (1997) Climate variability and climate change in Mexico: a review. *Geofísica Internacional* 36(3):201–205
- Jauregui E (1997) Heat island development in Mexico City. *Atmos Environ* 31(22):3821–3831. [https://doi.org/10.1016/S1352-2310\(97\)00136-2](https://doi.org/10.1016/S1352-2310(97)00136-2)
- Jauregui E, Romales E (1996) Urban effects on convective precipitation in Mexico city. *Atmos Environ* 30(20):3383–3389. [https://doi.org/10.1016/1352-2310\(96\)00041-6](https://doi.org/10.1016/1352-2310(96)00041-6)
- Joseph PV, Sooraj KP, Rajan CK (2006) The summer monsoon onset process over South Asia and an objective method for the date of monsoon onset over Kerala. *Int J Climatol* 26(13):1871–1893. <https://doi.org/10.1002/joc.1340>
- Klein SA, Soden BJ, Lau N-C (1999) Remote sea surface temperature variations during ENSO: evidence for a tropical atmospheric bridge. *J Clim* 12(4):917–932. [https://doi.org/10.1175/1520-0442\(1999\)012<0917:RSSTVD>2.0.CO;2](https://doi.org/10.1175/1520-0442(1999)012<0917:RSSTVD>2.0.CO;2)
- Lee J-Y, Wang B (2014) Future change of global monsoon in the CMIP5. *Clim Dyn* 42(1–2):101–119. <https://doi.org/10.1007/s00382-012-1564-0>
- Lerner AM, Eakin HC, Tellman E, Bausch JC, Hernández Aguilar B (2018) Governing the gaps in water governance and land-use planning in a megacity: the example of hydrological risk in Mexico City. *Cities* 83:61–70. <https://doi.org/10.1016/j.cities.2018.06.009>
- Lunneborg CE (1985) Estimating the correlation coefficient: the bootstrap approach. *Psychol Bull* 98(1):209–215. <https://doi.org/10.1037/0033-2909.98.1.209>
- Magaña V, Amador JA, Medina S (1999) The midsummer drought over Mexico and Central America. *J Clim* 12(6):1577–1588. [https://doi.org/10.1175/1520-0442\(1999\)012%3c1577:TMDOMA%3e2.0.CO;2](https://doi.org/10.1175/1520-0442(1999)012%3c1577:TMDOMA%3e2.0.CO;2)
- Magaña V, Pérez J, Méndez M (2003a) Diagnosis and prognosis of extreme precipitation events in the Mexico City basin. *Geofis Int* 42:247–260
- Magaña V, Vázquez J, Pérez J, Pérez J (2003b) Impact of El Niño on precipitation in Mexico. *Geofísica Internacional* 42(3):313–330
- Marengo JA, Liebmann B, Kousky VE, Filizola NP, Wainer IC (2001) Onset and end of the rainy season in the Brazilian Amazon Basin. *J Clim* 14(5):833–852. [https://doi.org/10.1175/1520-0442\(2001\)014%3c0833:OAEOTR%3e2.0.CO;2](https://doi.org/10.1175/1520-0442(2001)014%3c0833:OAEOTR%3e2.0.CO;2)
- Melgarejo, A., Ordoñez, P., Nieto, R., Gimeno, L., & Ribera, P. (2017). Moisture transport related to the ENSO effects in the Mexican precipitation. *Proc First Int Electron Conf Hydrological Cycle* 4884 <https://doi.org/10.3390/CHyCle-2017-04884>
- Méndez M, Magaña V (2010) Regional aspects of prolonged meteorological droughts over Mexico and Central America. *J Clim* 23(5):1175–1188. <https://doi.org/10.1175/2009JCLI3080.1>
- Mendoza B, Jáuregui E, Diaz-Sandoval R, García-Acosta V, Velasco V, Cordero G (2005) Historical droughts in Central Mexico and their relation with El Niño. *J Appl Meteorol* 44(5):709–716. <https://doi.org/10.1175/JAM2210.1>
- Misra V, Dixit S, Jayasankar CB (2023) The regional diagnosis of onset and demise of the rainy season over tropical and subtropical Australia. *Earth Interact* 27(1):220026. <https://doi.org/10.1175/EI-D-22-0026.1>
- Montero-Rosado C, Ojeda-Trejo E, Espinosa-Hernández V, Fernández-Reynoso D, Caballero Deloya M, Benedicto Valdés GS (2022) Water diversion in the Valley of Mexico Basin: an environmental transformation that caused the desiccation of Lake Texcoco. *Land* 11(4):542. <https://doi.org/10.3390/land11040542>
- NCEI (2022) Equatorial Pacific sea surface temperatures. <https://www.ncei.noaa.gov/access/monitoring/enso/sst/>. Last access: 23 November 2022
- Ochoa CA, Quintanar AI, Raga GB, Baumgardner D (2015) Changes in intense precipitation events in Mexico City. *J Hydrometeorol* 16(4):1804–1820. <https://doi.org/10.1175/JHM-D-14-0081.1>
- Omay PO, Muthama NJ, Oludhe C, Kinama JM, Artan G, Atheru Z (2023) Changes and variability in rainfall onset, cessation, and length of rainy season in the IGAD region of Eastern Africa. *Theoret Appl Climatol* 152(1–2):871–893. <https://doi.org/10.1007/s00704-023-04433-0>
- Oo K-T (2023). Climatology definition of the Myanmar Southwest Monsoon (MSwM): Change Point Index (CPI). Advances in Meteorology. Article ID 2346975, 18 pages <https://doi.org/10.1155/2023/2346975>
- Ordoñez P, Gallego D, Ribera P, Peña-Ortiz C, García-Herrera R (2016) Tracking the Indian summer monsoon onset back to the preinstrument period. *J Clim* 29(22):8115–8127. <https://doi.org/10.1175/JCLI-D-15-0788.1>
- Ordoñez P, Nieto R, Gimeno L, Ribera P, Gallego D, Ochoa-Moya CA, Quintanar AI (2019) Climatological moisture sources for the Western North American Monsoon through a Lagrangian approach: Their influence on precipitation intensity. *Earth Syst Dyn* 10(1):59–72. <https://doi.org/10.5194/esd-10-59-2019>
- Pai MN, Rajeevan MN (2009) Summer monsoon onset over Kerala: new definition and prediction. *J Earth Syst Sci* 118(2):123–135

- Perdigón-Morales J, Romero-Centeno R, Ordóñez P, Barrett BS (2018) The midsummer drought in Mexico: perspectives on duration and intensity from the CHIRPS precipitation database. *Int J Climatol* 38(5):2174–2186. <https://doi.org/10.1002/joc.5322>
- Perdigón-Morales J, Romero-Centeno R, Ordoñez P, Nieto R, Gimeno L, Barrett BS (2021) Influence of the Madden-Julian Oscillation on moisture transport by the Caribbean Low Level Jet during the Midsummer Drought in Mexico. *Atmos Res* 248:105243. <https://doi.org/10.1016/j.atmosres.2020.105243>
- Raju PVS, Mohanty UC, Bhatla R (2007) Interannual variability of onset of the summer monsoon over India and its prediction. *Nat Hazards* 42(2):287–300. <https://doi.org/10.1007/s11069-006-9089-7>
- Ramírez C (1990) El agua en la Cuenca de México. In: Kumate J, Mazari M (eds) Los problemas de la Cuenca de México. El Colegio Nacional, México, D.F., pp 61–82
- Rogé PSB (2013) Rainfed Agriculture and Climatic Variability in Oaxaca, Mexico. A dissertation submitted in partial satisfaction of the requirements for the degree of Doctor of Philosophy in Environmental Science, Policy, and Management in the Graduate Division of the University of California, Berkeley. <https://escholarship.org/uc/item/0zb469hm>.
- Schmitz JT, Mullen SL (1996) Water vapor transport associated with the summertime North American monsoon as depicted by ECMWF analyses. *J Clim* 9(7):1621–1634. [https://doi.org/10.1175/1520-0442\(1996\)009%3c1621:WVTAWT%3e2.0.CO;2](https://doi.org/10.1175/1520-0442(1996)009%3c1621:WVTAWT%3e2.0.CO;2)
- Vera C, Higgins W, Amador J, Ambrizzi T, Garreaud R, Gochis D, Gutierrez D, Lettenmaier D, Marengo J, Mechoso CR, Nogues-Paegle J, Dias PLS, Zhang C (2006) Toward a unified view of the American monsoon systems. *J Clim* 19(20):4977–5000. <https://doi.org/10.1175/JCLI3896.1>
- Wang C (2007) Variability of the Caribbean Low-Level Jet and its relations to climate. *Clim Dyn* 29(4):411–422. <https://doi.org/10.1007/s00382-007-0243-z>
- Wang B, Ding Q (2008) Global monsoon: dominant mode of annual variation in the tropics. *Dyn Atmos Oceans* 44(3–4):165–183. <https://doi.org/10.1016/j.dynatmoce.2007.05.002>
- Wang C, Lee S (2007) Atlantic warm pool, Caribbean low-level jet, and their potential impact on Atlantic hurricanes. *Geophys Res Lett* 34(2):L02703. <https://doi.org/10.1029/2006GL028579>
- Wang C, Lee S, Enfield DB (2007) Impact of the Atlantic warm pool on the summer climate of the Western Hemisphere. *J Clim* 20(20):5021–5040. <https://doi.org/10.1175/JCLI4304.1>
- Wang B, Ding Q, Joseph PV (2009) Objective definition of the Indian summer monsoon onset. *J Clim* 22(12):3303–3316. <https://doi.org/10.1175/2008JCLI2675.1>
- Wang B, Li J, Cane MA, Liu J, Webster PJ, Xiang B, Kim H-M, Cao J, Ha K-J (2018) Toward predicting changes in the land monsoon rainfall a decade in advance. *J Clim* 31(7):2699–2714. <https://doi.org/10.1175/JCLI-D-17-0521.1>
- Zeng X, Lu E (2004) Globally unified monsoon onset and retreat indexes. *J Clim* 17(11):2241–2248. [https://doi.org/10.1175/1520-0442\(2004\)017%3c2241:GUMOAR%3e2.0.CO;2](https://doi.org/10.1175/1520-0442(2004)017%3c2241:GUMOAR%3e2.0.CO;2)

Publisher's note Springer Nature remains neutral with regard to jurisdictional claims in published maps and institutional affiliations.